Physics-informed deep neural networks towards finite strain homogenization of unidirectional soft composites

Qiang Chen [a], Xiaoxiao Du [b,*], George Chatzigeorgiou [c], Fodil Meraghni [c], Gang Zhao [b], Zhibo Yang [a]

[a] *School of Mechanical Engineering, Xi'an Jiaotong University, Xi'an, 710049, Shaanxi, China*
[b] *School of Mechanical Engineering and Automation, Beihang University, Beijing, 100191, China*
[c] *Arts et Métiers Institute of Technology, CNRS, Université de Lorraine, LEM3-UMR7239, F-57000, Metz, France*

A B S T R A C T

The presence of heterogeneities and significant property mismatches in soft composites lead to complex behaviors that are challenging to model with conventional analytical or numerical homogenization techniques. The present work introduces a micromechanics-informed deep learning framework to characterize microscopic displacements and stress fields in soft composites with periodic microstructures undergoing finite deformation. The main obstacle we address is the construction of specific loss functions incorporating intricate knowledge of finite strain homogenization theory, which is valid for arbitrary macroscopic deformation gradients. Notably, a multi-network model is utilized to describe the discontinuities in material properties and solution fields within the composites. These neural networks communicate with each other through interface traction and displacement continuity conditions within the loss function. In addition, to exactly impose the periodicity boundary in hexagonal and square unit cells, the neural network architectures are modified by incorporating a number of trainable harmonic functions. A significant advantage of the current framework is that it allows for a straightforward solution of the governing partial differential equations expressed in terms of the first Piola-Kirchhoff stresses, eliminating the need for iterative formulations of the residual vector and tangent matrix required by classical numerical methods. We extensively assess the effectiveness of the proposed approach upon extensive comparison with isogeometric analysis to determine the displacement and Cauchy stress fields in square and hexagonal arrays of fibers/porosities, demonstrating neural networks as a powerful alternative to the conventional numerical approaches in finite deformation analysis of microstructural materials.

1. Introduction

Over the past few decades, new generations of advanced materials with complex microstructures have continued to be developed to meet specific application needs. Soft composites, like rubber-like materials, represent a unique class of materials that provide a cost-effective solution for broad engineering challenges. The demand to efficiently and accurately understand the homogenized behavior and underlying local responses of these microstructural materials contributed to the significant advancement of micromechanics theories. Amongst them, the finite-element/volume-based numerical methods (FEM/FVM) are widely accepted for solving unit cell problems generic to the analysis of periodic heterogeneous media that involve material or geometric nonlinearities (Khatam and Pindera, 2012; Saeb et al., 2016). This preference is due to the absence of analytical homogenization theories and the superior predictive capabilities of FEM/FVM techniques. These methods rely on constructing the residual vector and tangent matrix to form a nonlinear system of equations that needs to be solved iteratively (Kim, 2015), using techniques such as the Newton–Raphson method, to obtain nodal displacements at each load increment. The FEM and FVM techniques, however, come with several drawbacks such as mesh distortion in the case of large deformation analysis (Cavalcante and Pindera, 2013; Nazem and Moavenian, 2021), which may lead to numerical instabilities or inaccurate results.

Inspired by the success of deep learning techniques across various fields (Brodnik et al., 2023; El Fallaki Idrissi et al., 2024, 2025; Gajek et al., 2020), physically informed neural networks (PINNs) have recently gained recognition as a powerful method compared to traditional

* Corresponding author.
E-mail address: duxiaoxiao@buaa.edu.cn (X. Du).

numerical methods for discovering governing partial differential equations (PDEs) and identifying parameters (Karniadakis et al., 2021; Raissi et al., 2019). A key aspect of the PINN technique is its ability to incorporate not only measured (or reference data) but also the governing equations and the relevant initial and boundary conditions directly into the cost function, evaluated on selected material points, ensuring that the neural network's outputs comply with the system's physical laws. Moreover, the graph-based automatic differentiation in modern machine learning packages is exploited to efficiently evaluate the derivatives of the neural network functionals. This sets the PINN approach apart from other purely data-driven neural network methods that solely rely on minimizing the distance between the neural network outputs and reference data. In the theory of elasticity, two versions of the PINN technique exist in the literature, distinguished by how the loss function is constructed. The first version endows the neural network with the strong-form stress equilibrium or the linear momentum equations (Abueidda et al., 2021), while the second version directly addresses the total potential energy (Nguyen-Thanh et al., 2021; Samaniego et al., 2020). The training of the PINN is carried out by minimizing a cost function involving the PDE residuals or the total potential energy. The PINN framework has been successfully employed to obtain solutions in linear elasticity (Jiang et al., 2022), elastoplasticity (Haghighat et al., 2021; Roy et al., 2024), finite strain plasticity (Niu et al., 2023), viscoelasticity (Abueidda et al., 2022), hyperelasticity (Nguyen-Thanh et al., 2020), interface debonding (Tran et al., 2024) etc.

However, the vanilla PINN technique faces significant challenges in the solution of unit cell problems in composites, offering no clear advantage in comparison with physical models. The first issue lies in the intrinsic difficulty in constructing the neural network architecture that satisfies the governing equations while capturing the displacement and traction periodic boundary conditions. The loss function in the vanilla PINN contains multiple loss terms that correspond to the PDEs and periodicity conditions, producing a multi-objective optimization problem. Balancing these different loss terms is nontrivial in order to yield accurate unit cell solutions. While several attempts have been reported in the literature by modifying the boundary conditions to exactly describe the physics constraints of the unit cell in the network architecture, these efforts are limited to certain boundary conditions (Henkes et al., 2022; Ren and Lyu, 2024), suggesting that reformulation of the loss terms representing the boundary conditions is indeed needed for different loading directions. The second issue is that neural networks encounter significant convergence challenges when there are discontinuities in the solution fields. The neural networks exhibit low trainability, producing unreliable solutions for problems involving high stress or deformation gradients. This is particularly problematic for composite materials, where there is a substantial mismatch between the properties of the fiber and the matrix phases. In response to this limitation, many investigators introduced a finite-thickness artificial interphase that provides a gradual transition in modulus between the fiber and matrix phases (Henkes et al., 2022; Linghu et al., 2024). This, however, introduces a new problem. That is, the stress field across the fiber/matrix interface becomes falsely diffused when it should be sharply defined.

The physically informed deep homogenization neural network (DHN) framework, proposed by Jiang et al. (2023), Wu et al. (2023), Chen et al. (2025), and Zhao et al. (2025), provides a paradigm shift in the continuing evolution of the PINN approach for the micromechanics-based analysis of periodic heterogeneous microstructures in both two and three-dimensional spaces. This framework utilizes a two-scale decomposition of the field variable into averaged and microscopic components, with the local unit cell solution derived through neural networks under periodic boundary conditions. The DHN's significance lies in its innovative modification of neural network architectures by integrating a "periodic" layer composed of trainable sinusoidal functions; therefore, the neural network outputs precisely and consistently satisfy the periodic boundary condition, which remains valid under the arbitrary combination of macroscopic strains. The DHN has proven highly effective in predicting microscopic field variables, as well as effective behavior when compared to classical numerical methods. To the authors' knowledge, no existing neural network-based homogenization models in the literature offer both the capability to handle arbitrary combinations of macroscopic strains and the local field accuracy achieved by the DHN theory. Data-driven, thermodynamics-consistent artificial neural networks (TANNs), which focus on training the free energy and enforcing thermodynamic laws, have also been developed for modeling the constitutive behavior of materials and the macroscopic response of composites, particularly within a multiscale framework (El Fallaki Idrissi et al., 2024; Masi and Stefanou, 2022, 2023; Masi et al., 2021; Sekkal et al., 2025). The key distinction between TANNs and the DHN method lies in their formulation: TANNs efficiently capture the homogenized behavior and local fields of composites, but they require supervised learning with labelled data. In contrast, the DHN method directly solves the strong-form governing PDEs to predict detailed microscale field distributions without relying on any labelled data. However, the DHN prevents the direct application within a multiscale framework, where the unit cell solution needs to be trained online at every integration point, would be computationally impractical.

In this study, the micromechanics-informed DHN theory is further extended by developing a finite strain framework for predicting microscopic displacement and stress distributions in soft composites with periodic microstructures. Unlike our earlier approach, which was limited to infinitesimal strain formulations, this work incorporates finite strain kinematics, significantly broadening its applicability to highly deformable materials. Additionally, we introduce a multi-network architecture, where distinct neural networks are employed for each phase of the composite—a crucial improvement that enhances the model's ability to capture solution discontinuities across the fiber/matrix interface. These neural networks are seamlessly connected via the interface traction and displacement continuity conditions within the neural network loss function. Periodic boundary conditions are precisely enforced using trainable sinusoidal functions, while the strong-form equilibrium equations, expressed in terms of the first Piola-Kirchhoff stresses, are directly integrated into the common loss function.

We validate the extended DHN framework with the isogeometric analysis (IGA) (Du et al., 2024; Hughes et al., 2005) for unidirectional composites consisting of elastic fibers that are ten times stiffer than the soft matrix or contain a hole. The results demonstrate the extended theory's ability to accurately capture local field distributions across a range of periodic microstructures and loading scenarios.

2. Finite-deformation homogenization theory

The objective of this section is focused on introducing the homogenization technique for large deformation analysis of heterogeneous hyperelastic materials. Thereafter, some preliminary notes concerning the Lagrangian framework and the periodic homogenization theory are recalled.

2.1. Preliminaries: Lagrangian framework

Consider a hyperelastic solid. Under finite deformation, the position of a material point in the deformed state $\mathbf{x}(\mathbf{X})$ can be represented with respect to its position in the undeformed state, $\mathbf{X}$, and displacement of this material particle, $\mathbf{u}(\mathbf{X})$, in the undeformed configuration, represented in Cartesian coordinates as follows:

$$\mathbf{x}(\mathbf{X}) = \mathbf{X} + \mathbf{u}(\mathbf{X}) \tag{1}$$

Accordingly, the component of the deformation tensor $\mathbf{F}$ reads:

$$F_{ij} = \frac{\partial x_i}{\partial X_j} = \frac{\partial u_i}{\partial X_j} + \delta_{ij} = H_{ij} + \delta_{ij} \tag{2}$$

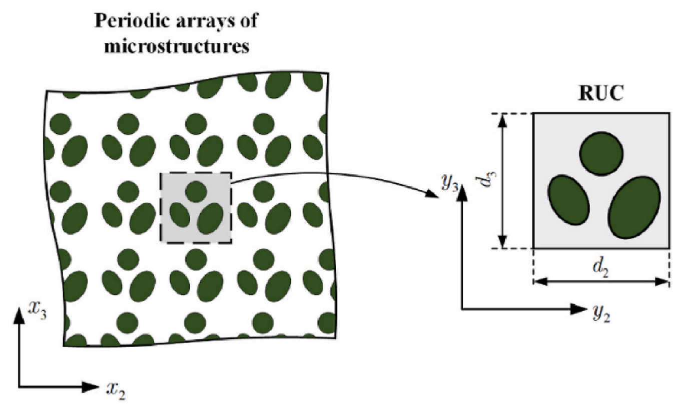

Fig. 1. Characterization of periodic heterogeneous media using RUC.

where $H_{ij} = \partial u_i / \partial X_j$ represents displacement gradient. δ_{ij} denotes Kronecker delta.

The right Cauchy-Green symmetric deformation tensor **C**, employed in the formulation of potential-based constitutive equations, is expressed as:

$$\mathbf{C} = \mathbf{F}^{\mathrm{T}}\mathbf{F} \tag{3}$$

The second Piola-Kirchhoff symmetric stress tensor **S** can be expressed in terms of the chosen strain-energy density function W and the right Cauchy-Green deformation tensor **C** as follows:

$$S_{ij} = 2\frac{\partial W}{\partial C_{ij}} \tag{4}$$

It is worth noting that while the second Piola-Kirchhoff stress tensor **S** has been widely used in classical numerical solutions for large deformation problems due to its symmetric properties, the proposed neural network approach instead employs the unsymmetric first Piola-Kirchhoff stress tensor **T**, defined in Eq. (5), for homogenization. This is because the first Piola-Kirchhoff stress is conjugate to the deformation gradient, whereas the second Piola-Kirchhoff stress is conjugate to the Green-Lagrange strain. A proper Hill-Mandel condition cannot be established using the Green-Lagrange strain, as its average does not correspond to the macroscopic one, as demonstrated by Nemat-Nasser (1999).

$$\mathbf{T} = \mathbf{S}\mathbf{F}^{\mathrm{T}} = J\mathbf{F}^{-1}\boldsymbol{\sigma} \tag{5}$$

where $\boldsymbol{\sigma}$ denotes the Cauchy stress and $J = \det(\mathbf{F})$.

In the state of equilibrium without inertia effect, the governing differential equations of the hyperelastic solid can be formulated using the first Piola-Kirchhoff stress **T** as follows:

$$\frac{\partial T_{ij}}{\partial X_i} = 0 \tag{6}$$

2.2. Unit cell solutions

As illustrated in Fig. 1, we consider a periodic array of unidirectional fiber/porosity in the matrix phase. The behavior of the entire array can be accurately captured by its smallest fundamental component, often referred to in the literature as the repeating unit cell (RUC), under periodic boundary conditions. Following the computational homogenization theory (Bensoussan et al., 1978; Chen and Pindera, 2020; Chen et al., 2018; Cruz-González et al., 2020; Suquet, 1987), the displacement field u_i in each phase of the composites can be obtained as the two-scale representation that includes both averaged and fluctuating contributions, depending on the global **X** and local **y** position (coordinates) in the undeformed state, respectively:

$$u_i(\mathbf{X}, \mathbf{y}) = \overline{H}_{ij}X_j + u_i'(\mathbf{y}) \tag{7}$$

where, $i = 1, 2, 3$. $\overline{H}_{ij}$ indicates macroscopic displacement gradient. u_i' denotes the fluctuating displacement due to the presence of the micro-

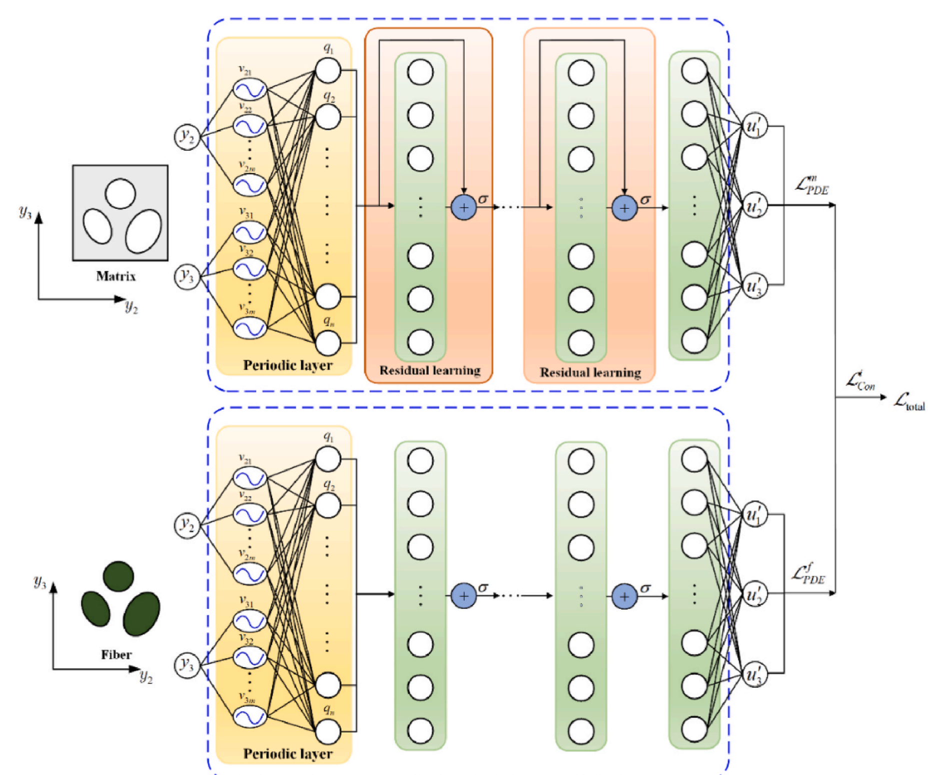

Fig. 2. Surrogate model for the finite deformation analysis of periodic microstructures using deep learning.

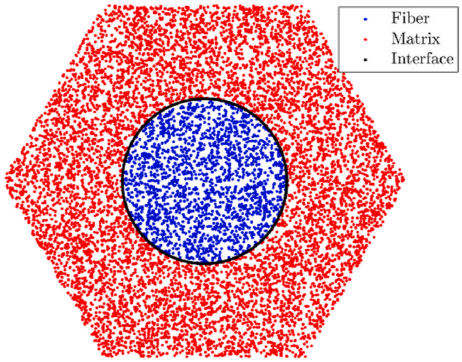

Fig. 3. Distribution of material points in the hexagonal unit cell used in the loss function. The fiber contains 2000 material points, the matrix has 8000 material points, and the interface includes 360 material points.

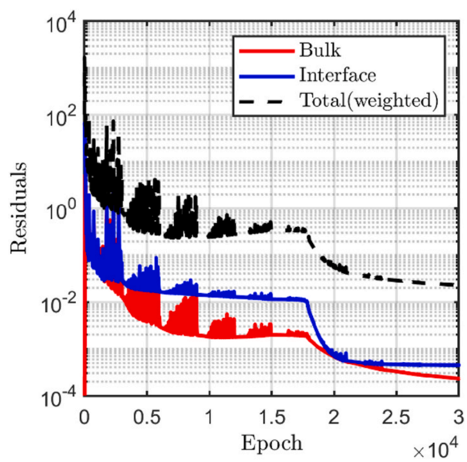

Fig. 4. Comparison of interface and bulk loss with respect to training epochs.

structures. The components of the deformation gradient F_{ij} are then expressed as:

$$F_{ij} = \overline{F}_{ij} + H'_{ij} = \overline{H}_{ij} + \delta_{ij} + \frac{\partial u'_i}{\partial y_j} \tag{8}$$

where $\overline{F}_{ij} = \overline{H}_{ij} + \delta_{ij}$ indicates the macroscopic deformation gradient and $H'_{ij} = \partial u'_i / \partial y_j$ denotes the fluctuating displacement gradient. Particularly, for unidirectional fiber or porosity aligned parallel to the y_1 axis, considering the generalized plane "strain" assumption ($\partial u'_i / \partial y_1 \equiv 0$), the deformation tensor can be reformulated in the matrix form:

$$\mathbf{F} = \begin{bmatrix} 1+\overline{H}_{11} & \overline{H}_{12}+H'_{12} & \overline{H}_{13}+H'_{13} \\ \overline{H}_{21} & 1+\overline{H}_{22}+H'_{22} & \overline{H}_{23}+H'_{23} \\ \overline{H}_{31} & \overline{H}_{32}+H'_{32} & 1+\overline{H}_{33}+H'_{33} \end{bmatrix} \tag{9}$$

The complex material responses for the matrix and fiber phases can be characterized using the generalized Mooney-Rivlin (GMR) materials (Du et al., 2020; Khatam and Pindera, 2012). The GMR model is well-suited for modeling soft media due to its versatile control over compressibility. The strain energy density function of the GMR model reads:

$$W = c_1\left(\frac{I_1}{I_3^{1/3}} - 3\right) + c_2\left(\frac{I_2}{I_3^{2/3}} - 3\right) + \frac{\kappa}{2}(J-1)^2 \tag{10}$$

where $I_1 = \mathrm{tr}\mathbf{C}$, $I_2 = \frac{1}{2}\left(\mathrm{tr}^2\mathbf{C} - \mathrm{tr}\mathbf{C}^2\right)$ and $I_3 = \det\mathbf{C}$ are the three invariants of the right Cauchy-Green deformation tensor $\mathbf{C}$ in Eq. (3). $J = \det\mathbf{F} = \sqrt{I_3}$. c_1, c_2, κ are material constants, with $c_1 + c_2 = \mu/2$ and μ and κ denote shear and bulk moduli, respectively. It is noted that the GMR model can be reduced to compressible neo-Hookean in the case of $c_2 = 0$.

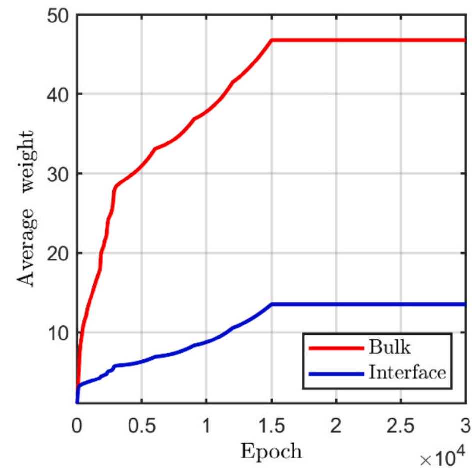

Fig. 5. Comparison of average interface and bulk collocation point weights with respect to training epochs.

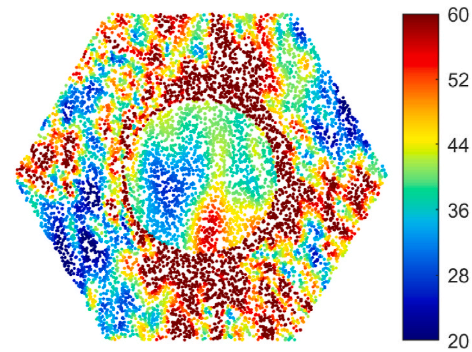

Fig. 6. Pointwise weight distributions of the trained network.

Using the above strain-energy density function, the second Piola-Kirchhoff symmetric stress tensor $\mathbf{S}$ can be calculated according to:

$$S_{ij} = 2\left(W_1\frac{\partial I_1}{\partial C_{ij}} + W_2\frac{\partial I_2}{\partial C_{ij}} + W_3\frac{\partial I_3}{\partial C_{ij}}\right) \tag{11}$$

where $W_1 = c_1/I_3^{1/3}$, $W_2 = c_2/I_3^{2/3}$, $W_3 = -\frac{1}{3}c_1 I_1/I_3^{4/3} - \frac{2}{3}c_2 I_2/I_3^{5/3} + \frac{1}{2}\kappa\left(1 - 1/I_3^{1/2}\right)$.

The above equations are then utilized in the evaluation of the first Piola-Kirchhoff stress $\mathbf{T} = \mathbf{S}\mathbf{F}^{\mathrm{T}}$ through Eq. (5) and then the equilibrium equations in Eq. (6). Additionally, at the fiber/matrix interface, the following continuity conditions hold:

$$\begin{aligned} u'_i\big|_f &= u'_i\big|_m, \\ t_i\big|_f + t_i\big|_m &= 0 \end{aligned} \tag{12}$$

where $t_i = T_{ij}n_j$ is the traction-like variable. n_i denotes the component of the outward unit normal vector in the undeformed configuration. $\cdot|_{(f,m)}$ indicates the displacement or traction component evaluated along the fiber/matrix interface. Along the unit cell exterior faces S, the periodicity conditions must be maintained:

$$\begin{aligned} u_i(\mathbf{x}_o + \mathbf{d}) &= u_i(\mathbf{x}_o) + \overline{H}_{ij}d_j, \\ t_i(\mathbf{x}_o + \mathbf{d}) + t_i(\mathbf{x}_o) &= 0 \end{aligned} \tag{13}$$

where $(\mathbf{x}_o, \mathbf{x}_o + \mathbf{d}) \in S$, $\mathbf{d} = [d_2, d_3]$ denote widths of the unit cell in y_2

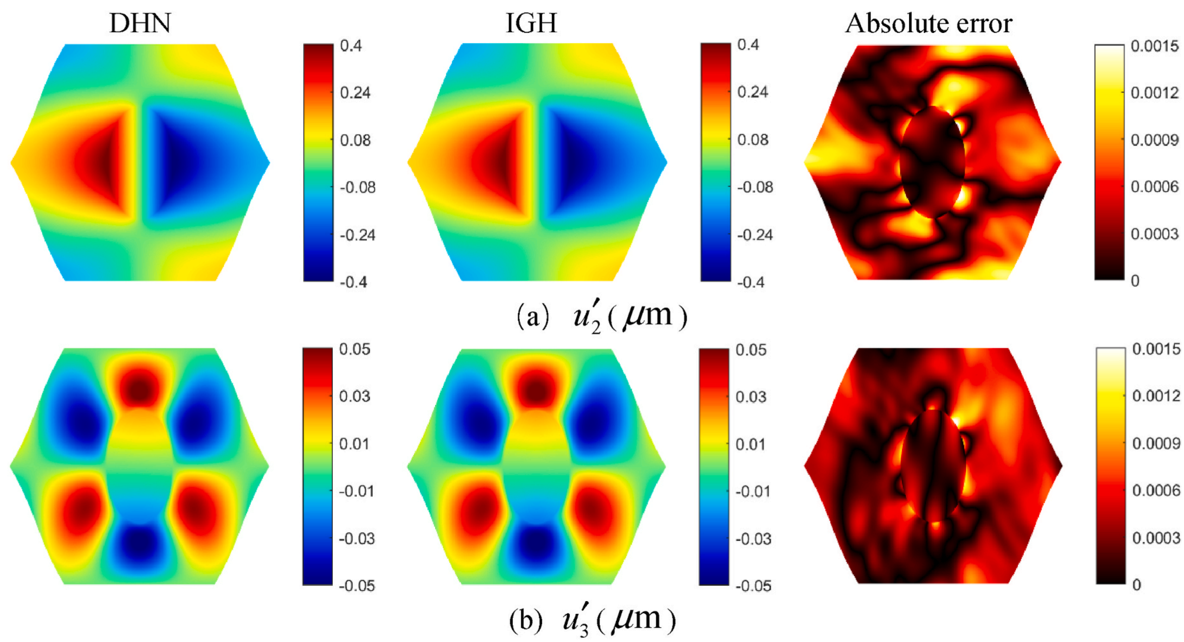

Fig. 7. Comparison of fluctuating displacement u_2', u_3' distributions in hexagonal array of unidirectional fiber generated with the DHN and IGH method under macroscopic displacement gradient $\overline{H}_{22} = 0.5$

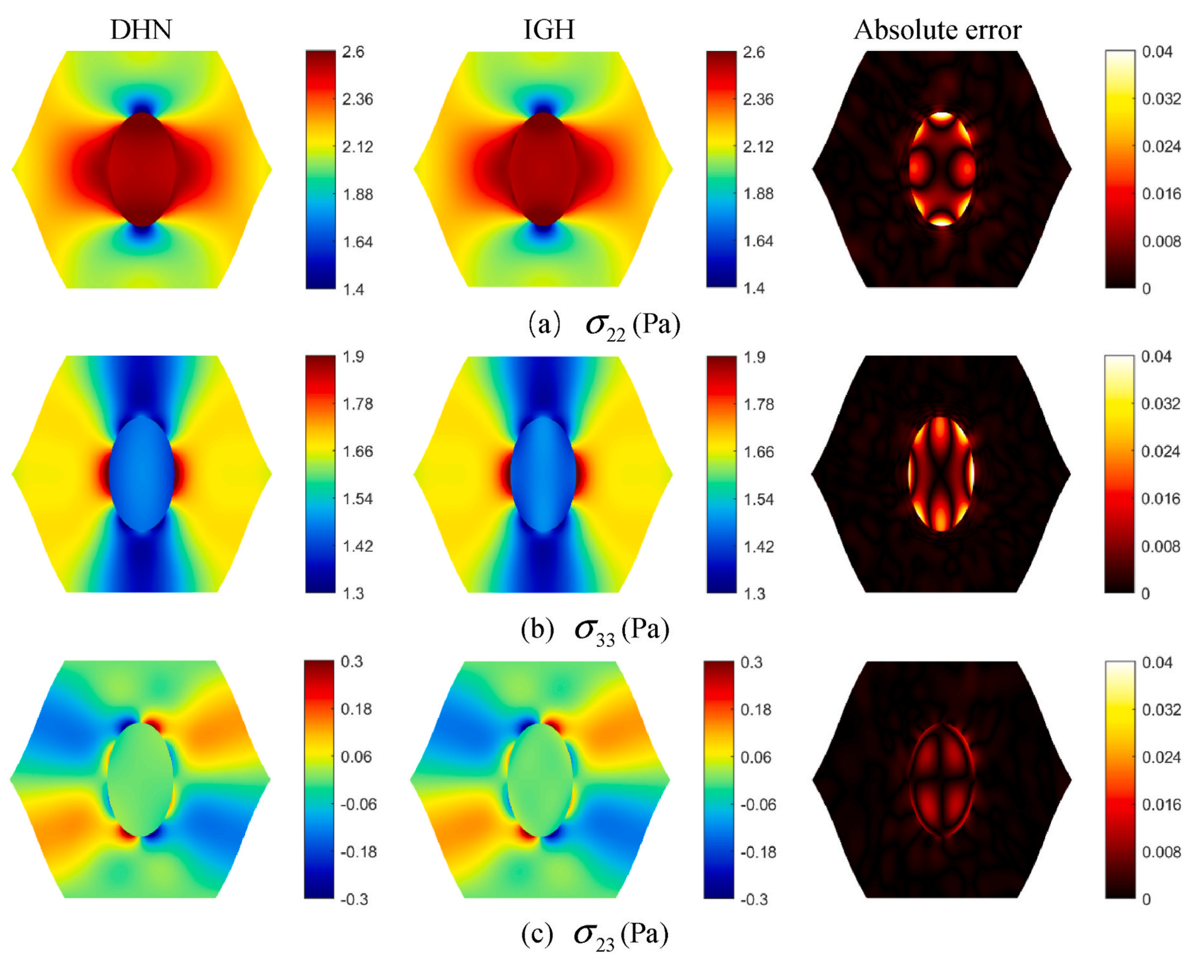

Fig. 8. Comparison of transverse normal σ_{22}, σ_{33} and shear σ_{23} stress distributions in hexagonal array of unidirectional fiber generated with the DHN and IGH method under macroscopic displacement gradient $\overline{H}_{22} = 0.5$

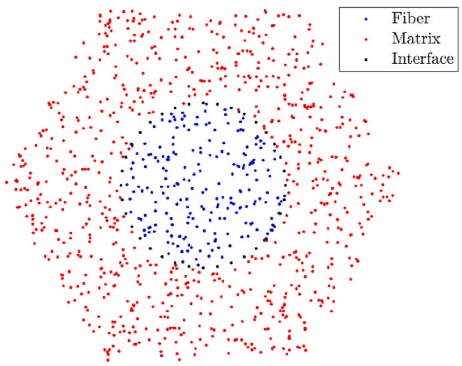

Fig. 9. Coarse distribution of material points, demonstrating the effect of collocation point density on the neural network accuracy. The fiber contains 214 material points, the matrix has 797 material points, and the interface includes 36 material points.

and y_3 directions, respectively.

3. Finite strain deep homogenization theory

As illustrated in Fig. 2, within the finite deformation framework, the objective is to develop a multi-network model, $\mathcal{N}\mathcal{N}$ that relates the spatial coordinates within the fiber and matrix domains to the fluctuating displacements of the RUC under given macroscopic deformation gradient $\overline{F}_{ij}$, with the known strain-energy density function W, as follows:

$$[u_1', u_2', u_3']^{(k)} = \underset{W,\overline{F}_{ij}}{\mathcal{N}\mathcal{N}}[y_2, y_3]^{(k)} \tag{14}$$

where $k = f, m$ represents the fiber or the matrix phase. Particularly, the deep neural networks in the matrix phase consist of several residual layers, where the inputs q_j^{l-1} and outputs q_j^l of the lth layer are transmitted through the network as follows:

$$q_j^l = g\left(w_{i,j}^l q_j^{l-1} + b_j^l + q_j^{l-1}\right) \tag{15}$$

In the equation above, $w_{i,j}^l$ and b_j^l denote the weights and biases of the lth layer, respectively. g signifies the nonlinear activation function. Conversely, residual layers cannot be used in the fiber phase due to sudden explosions in the training loss. Instead, only fully connected

boundary conditions, ensuring compliance with the physical laws. In the first place, to ensure the exact fulfillment of the periodicity characteristics of the RUC, the neural network architecture is modified by incorporating a set of sinusoidal functions (Dong and Ni, 2021). Towards this end, the spatial coordinates (y_2, y_3) are transformed to:

$$\left(\frac{2\pi}{d_2}y_2, \frac{2\pi}{d_3}y_3\right) \rightarrow (y_2', y_3') \tag{16}$$

for square arrays of fibers/porosities, d_2 and d_3 define the periods of the unit cell in pertinent directions, and

$$\left(\frac{4\pi}{\sqrt{3}L}y_2, \frac{2\pi}{\sqrt{3}L}y_2 + \frac{2\pi}{L}y_3\right) \rightarrow (y_2', y_3') \tag{17}$$

for hexagonal arrays of fibers/porosities, L denotes the width of each side of the hexagon. The modified coordinates transformed using a series of harmonic functions with specified periods and adjustable parameters (Dong and Ni, 2021), ensure that the network predictions fully comply with the periodicity boundary conditions with the desired level of accuracy.

$$\begin{aligned}
v_{2i}(y_2) &= g\left[A_{2i}\cos(y_2' + \phi_{2i}) + c_{2i}\right],\\
v_{3i}(y_3) &= g\left[A_{3i}\cos(y_3' + \phi_{3i}) + c_{3i}\right],\\
q_j(y_2, y_3) &= g\left[\sum_{i=1}^{m} v_{2i}(y_2)W_{ij}^{(2)} + \sum_{i=1}^{m} v_{3i}(y_3)W_{ij}^{(3)} + B_j\right]
\end{aligned} \tag{18}$$

In the above equation, $1 \le i \le m$ and $1 \le j \le n$, m and n are the number of neurons in the $(j-1)$th and jth layer respectively. A_{2i}, A_{3i}, ϕ_{2i}, ϕ_{3i}, c_{2i}, c_{3i}, $W_{ij}^{(2)}$, $W_{ij}^{(3)}$ and B_j indicate the training parameters in the neural networks. Notably, the anti-periodicity of the traction vector is inherently satisfied, as the partial derivatives of the neural network outputs—used to evaluate the displacement gradient and traction vector—remain periodic due to the chosen harmonic functions and activation functions.

The fluctuating displacements $[u_1', u_2', u_3']^{(k)}$ are then determined by minimizing a cost function, which incorporates residuals of the PDEs along with interfacial continuity conditions for displacements and tractions:

$$\mathcal{L} = \mathcal{L}_{PDE} + \mathcal{L}_{Con} \tag{19}$$

where

$$\mathcal{L}_{PDE} = \frac{1}{N_b}\sum_{e=1}^{N_b}\lambda_{PDE}^e\left[\left(\frac{\partial T_{21}}{\partial y_2} + \frac{\partial T_{31}}{\partial y_3}\right)^2 + \left(\frac{\partial T_{22}}{\partial y_2} + \frac{\partial T_{32}}{\partial y_3}\right)^2 + \left(\frac{\partial T_{23}}{\partial y_2} + \frac{\partial T_{33}}{\partial y_3}\right)^2\right]\Bigg|_{(y_2^e, y_3^e)} \tag{20}$$

layers are employed. It is important to note that in our earlier work, we utilized a single neural network to approximate solutions for the entire unit cell. Since fully connected layers alone cannot accurately capture the abrupt changes in fiber/matrix properties and stress concentration at the interface in composite materials, we introduced a finite-thickness interphase with smoothly varying properties to address these challenges. Consequently, this approach smoothed out the stress concentration near the fiber/matrix interface, resulting in less precise stress distributions. The multi-network model proposed here, however, effectively overcomes these drawbacks and delivers a more accurate description of the microscopic variables.

The fluctuating displacements $[u_1', u_2', u_3']^{(k)}$ are determined by minimizing a cost function that incorporates the stress equilibriums and

$$\mathcal{L}_{Con} = \frac{1}{N_i}\sum_{e=1}^{N_i}\lambda_{Con}^e\left[[\![t_1]\!]^2 + [\![t_2]\!]^2 + [\![t_3]\!]^2 + [\![u_1']\!]^2 + [\![u_2']\!]^2 + [\![u_3']\!]^2\right]\Big|_{(y_1^e, y_2^e, y_3^e)} \tag{21}$$

where N_b and N_i represent the number of material points within the bulk materials of the unit cell and on the fiber/matrix interface that enter the cost function, respectively. For displacement components, $[\![\{\cdot\}]\!] = \{\cdot\}^f - \{\cdot\}^m$ and for traction components $[\![\{\cdot\}]\!] = \{\cdot\}^f + \{\cdot\}^m$, which ensure the satisfaction of continuity conditions at the matrix-fiber interfaces. λ_{PDE}^e and λ_{Con}^e are adjustable weights associated with each material point.

Eventually, to obtain the solutions of the fluctuating displacements

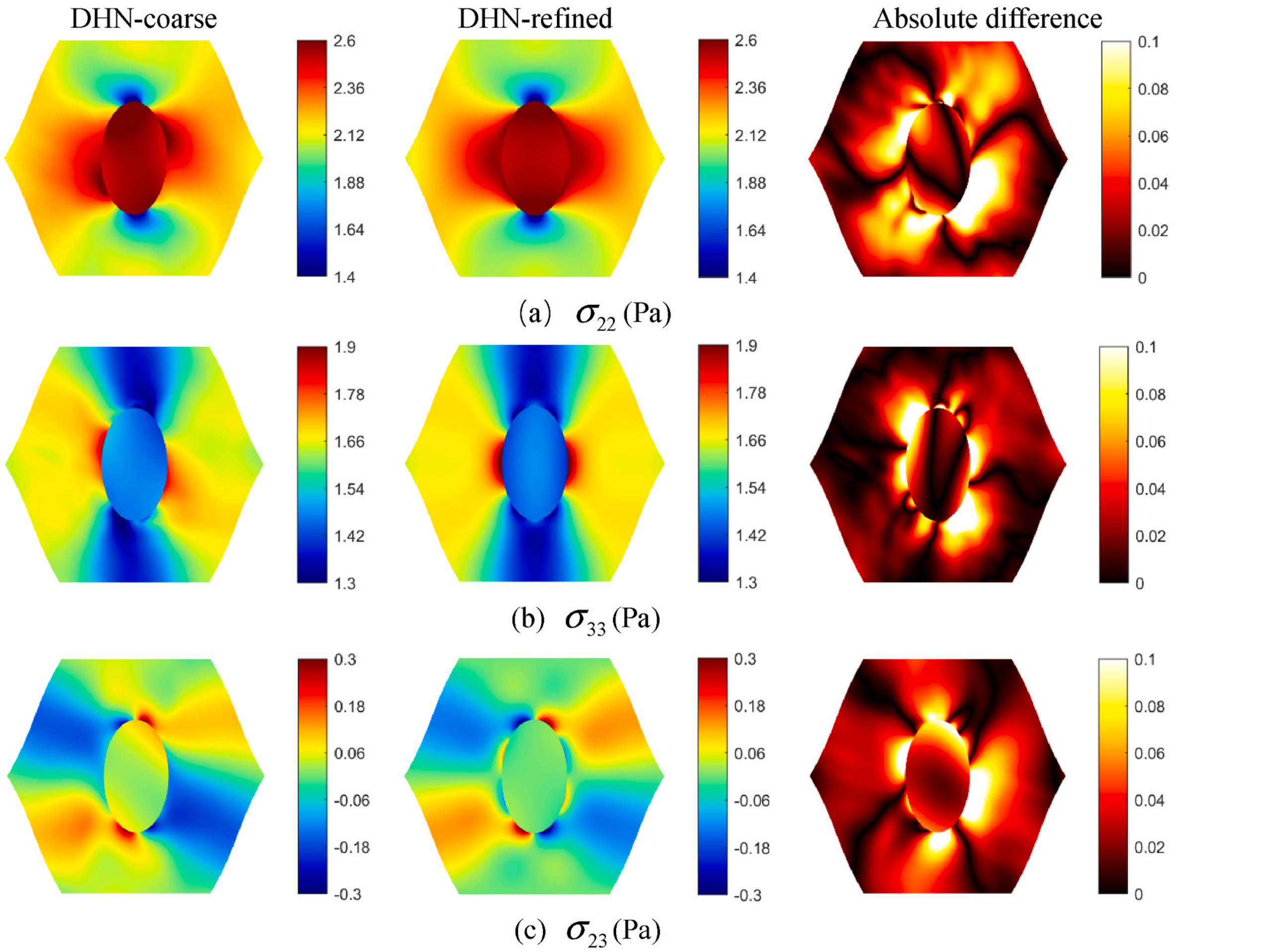

Fig. 10. Comparison of transverse normal σ_{22}, σ_{33} and shear σ_{23} stress distributions in hexagonal array of unidirectional fiber generated with the coarse and refined collocation points under macroscopic displacement gradient $\overline{H}_{22} = 0.5$

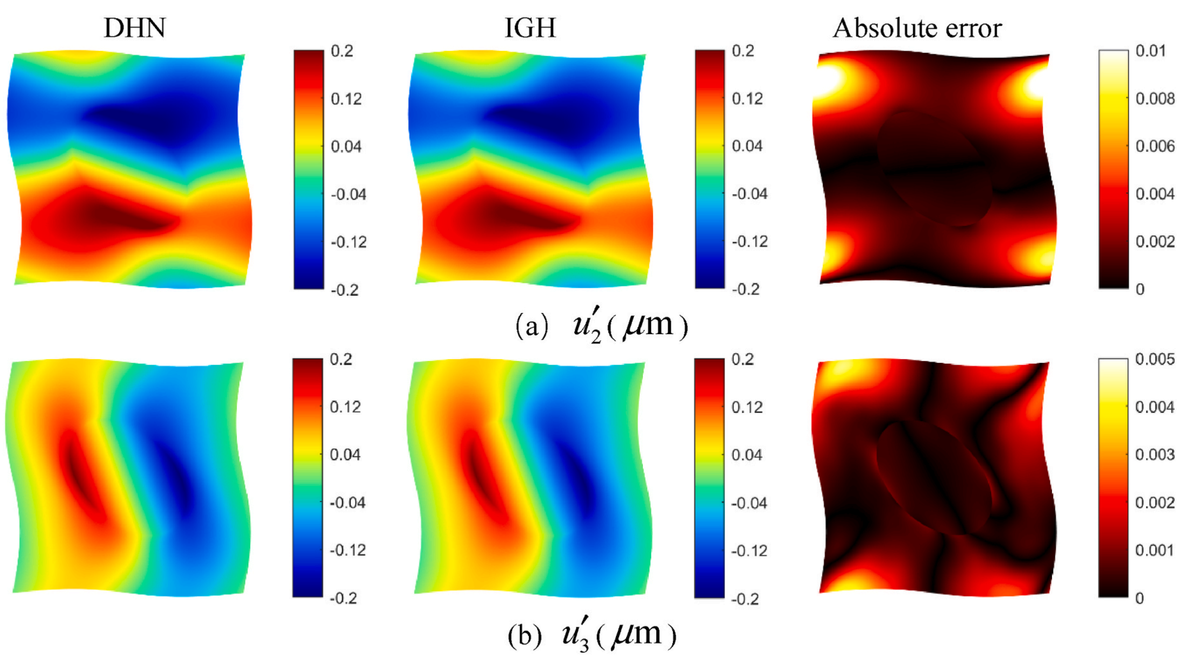

Fig. 11. Comparison of fluctuating displacement u_2', u_3' distributions in square array of unidirectional fiber with 20% fiber content generated with the DHN and IGH method under macroscopic displacement gradient $\overline{H}_{23} = 0.5$

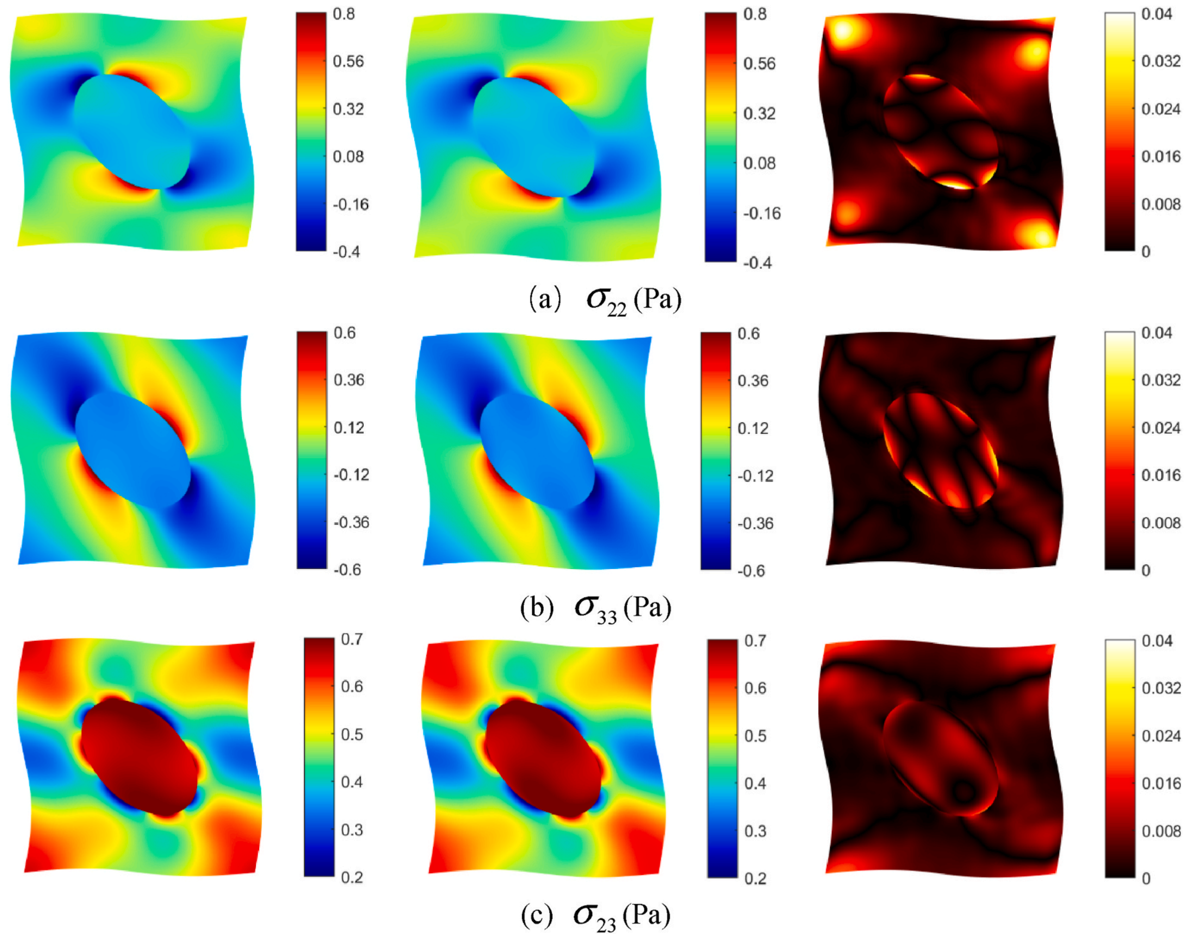

Fig. 12. Comparison of transverse normal σ_{22}, σ_{33} and shear σ_{23} stress distributions in square array of unidirectional fiber with 20% fiber content generated with the DHN and IGH method under macroscopic displacement gradient $\overline{H}_{23} = 0.5$

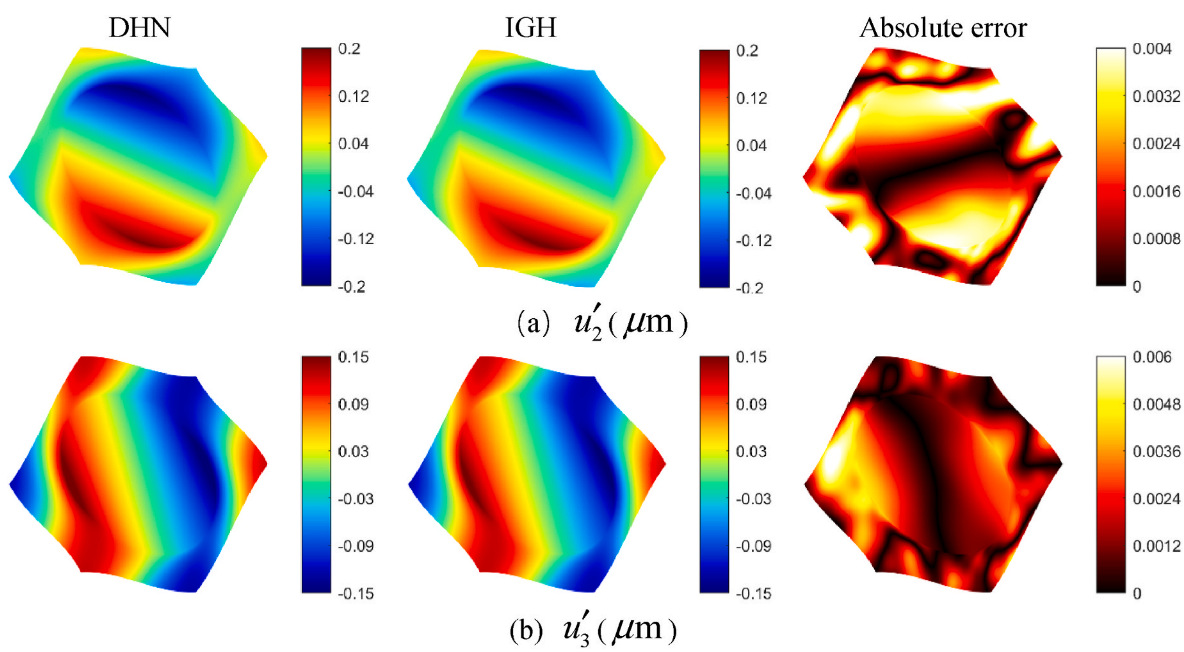

Fig. 13. Comparison of fluctuating displacement u'_2, u'_3 distributions in hexagonal array of unidirectional fiber with 50% fiber content generated with the DHN and IGH method under macroscopic displacement gradient $\overline{H}_{23} = 0.5$

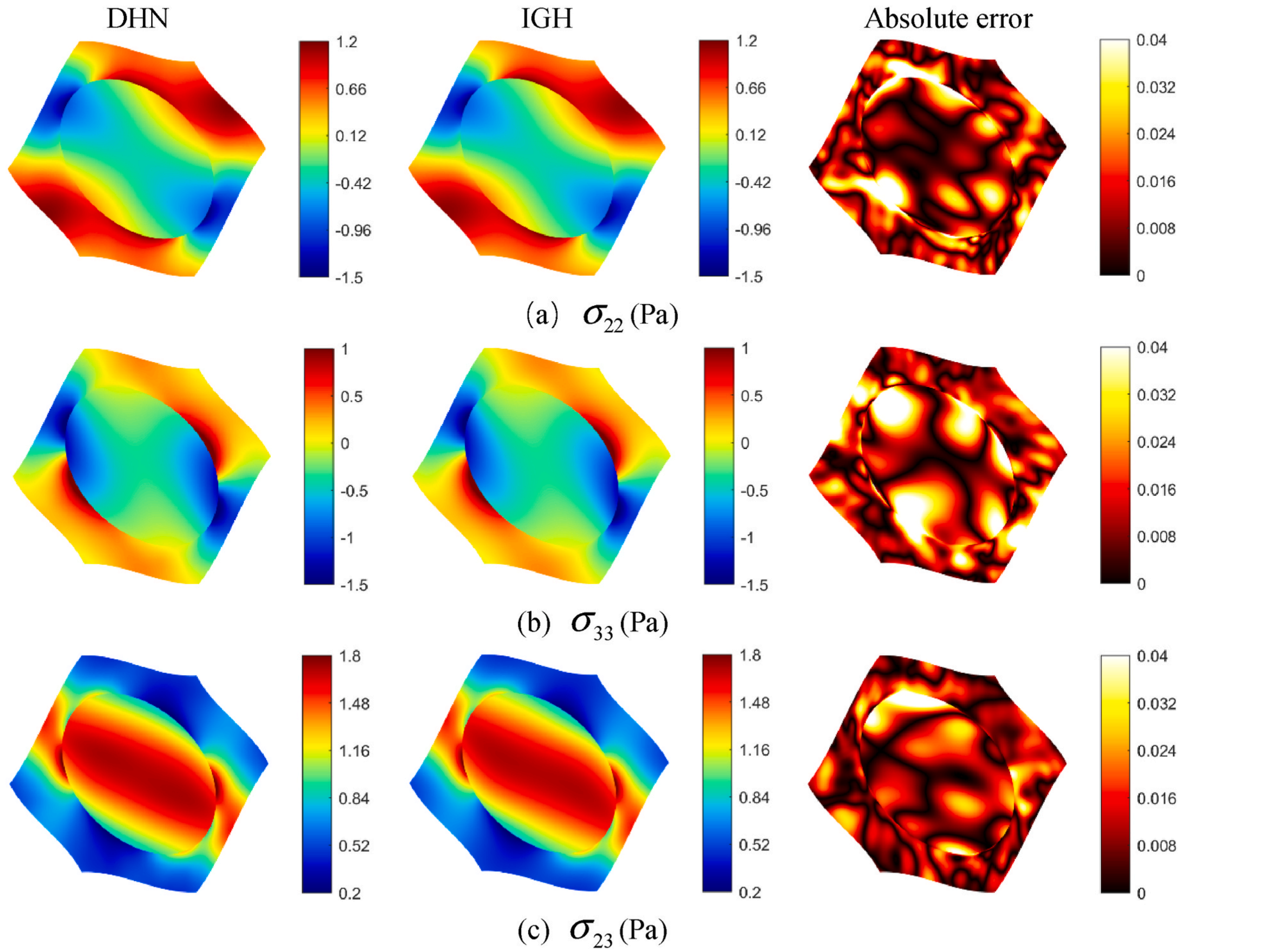

Fig. 14. Comparison of transverse normal σ_{22}, σ_{33} and shear σ_{23} stress distributions in hexagonal array of unidirectional fiber with 50% fiber content generated with the DHN and IGH method under macroscopic displacement gradient $\overline{H}_{23} = 0.5$

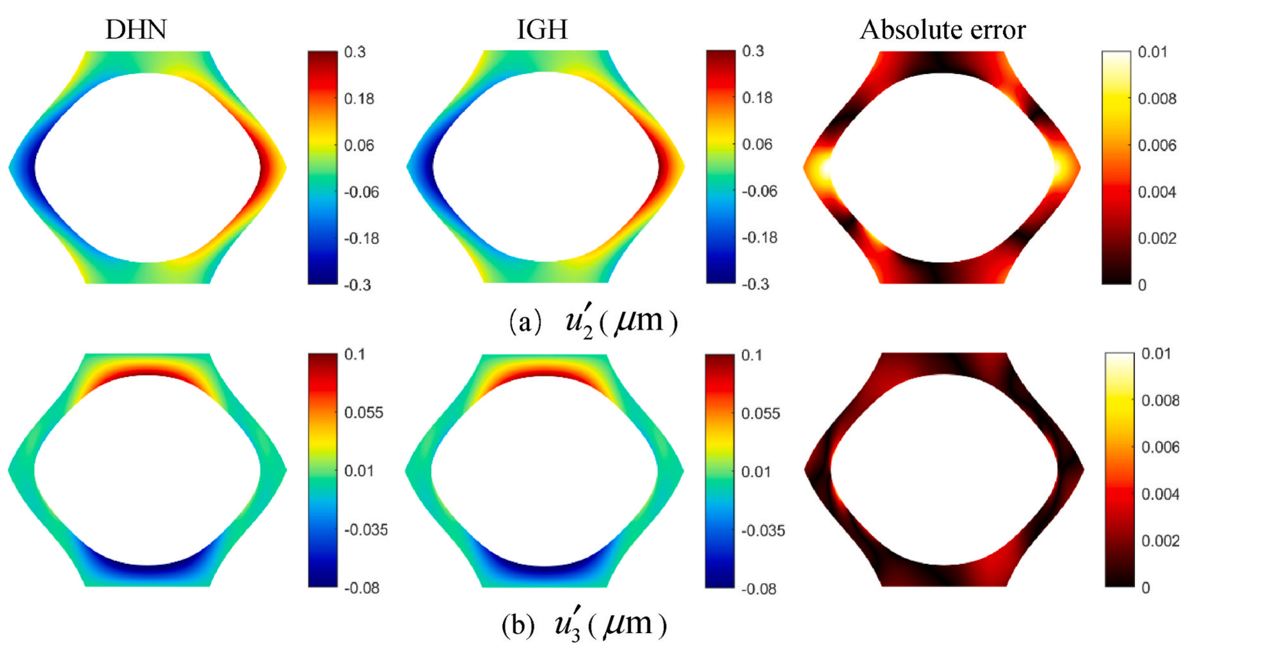

Fig. 15. Comparison of fluctuating displacement u_2', u_3' distributions in hexagonal array of unidirectional pore with 50% pore content generated with the DHN and IGH method under macroscopic displacement gradient $\overline{H}_{22} = 0.5$

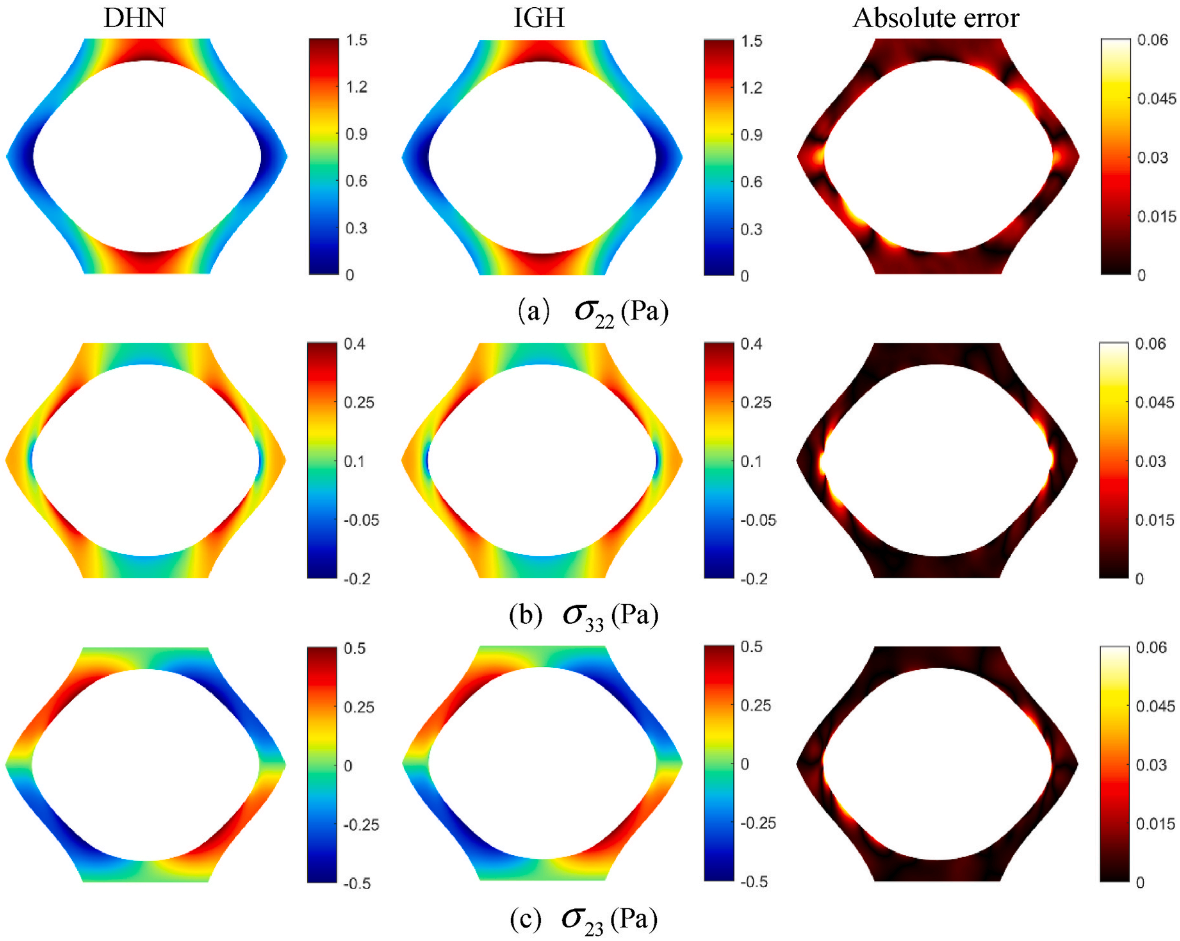

Fig. 16. Comparison of transverse normal σ_{22}, σ_{33} and shear σ_{23} stress distributions in hexagonal array of unidirectional pore with 50% pore content generated with the DHN and IGH method under macroscopic displacement gradient $\overline{H}_{22} = 0.5$

under given macroscopic deformation gradients, we minimize the overall loss $\mathscr{L}$ with respect to the network parameters $\mathbf{\theta}$ by utilizing gradient descent. Simultaneously, we seek to maximize the total loss function $\mathscr{L}$ with respect to the adaptive weights using gradient ascent λ^e_{PDE} and λ^e_{Con} by applying gradient ascent according to (McClenny and Braga-Neto, 2023; Wu et al., 2024):

$$\begin{aligned}
\mathbf{\theta}^{k+1} &= \mathbf{\theta}^k - \eta_k \nabla_{\mathbf{\theta}} \mathscr{L}, \\
\mathbf{\lambda}^{k+1}_{PDE} &= \mathbf{\lambda}^k_{PDE} + \rho^k_{PDE} \nabla_{\lambda PDE} \mathscr{L}, \\
\mathbf{\lambda}^{k+1}_{Con} &= \mathbf{\lambda}^k_{Con} + \rho^k_{Con} \nabla_{\lambda_{Con}} \mathscr{L}
\end{aligned} \tag{22}$$

where $\mathbf{\theta} = \left\{A_{2i}, A_{3i}, \phi_{2i}, \phi_{3i}, c_{2i}, c_{3i}, W^{(2)}_{ij}, W^{(3)}_{ij}, B_j, w^l_{i,j}, b^l_j\right\}$, η_k represents the learning rate for the network parameters $\mathbf{\theta}$ at the kth step. $\rho^k_{(\cdot)}$ is a distinct learning rate associated with the adaptive weights.

4. Numerical results

In this section, we aim to validate the accuracy of the developed finite deformation deep homogenization theory through comparison with the in-house isogeometric homogenization technique (IGH) (Chen et al., 2023; Du et al., 2024). This comparison focuses on predicting the local field variable distributions in unidirectional periodic composites/porous media under various loading conditions and volume fractions. To equitably compare the IGH and DHN methods, the identical periodic micromechanics framework is utilized for both approaches. Specifically, the displacement field is expressed in terms of averaged and microscopic contributions, and the microscopic problem is solved subject to periodic constraints. In what follows, the material properties, taken directly from Khatam and Pindera (2012), were employed in generating the results that follow. Namely, the matrix is modelled as a GMR material with parameters of $c_1 = 0.3$ Pa, $c_2 = 0.1$ Pa and $\kappa = 3.0$ Pa, which correspond to initial Young's modulus of $E = 2.204$Pa and Poisson's ratio of $\nu = 0.38$. In contrast, to mimic linear fiber, the parameters for the fiber phase are set to $c_1 = 4.408$ Pa, $c_2 = 0.0$ Pa and $\kappa = 14.69$ Pa, which yield an initial Young's modulus of $E = 22.04$ Pa, and Poisson's ratio of $\nu = 0.25$. The fiber/pore radius is 1μm. Note that the parameters of the fiber are ten times stiffer than those of the matrix. The considerable difference in material properties causes substantial stress concentrations around the interface, thus presenting a thorough and challenging evaluation of the accuracy of the proposed neural network method.

It should be emphasized that we focus on a unit cell with a single inclusion because the proposed DHN method does not demonstrate a clear advantage over classical numerical methods for unit cells containing randomly distributed inclusions, in terms of computational efficiency and accuracy. Due to the sharp stress and deformation gradients in such configurations, the neural network struggled to converge to accurate solutions during training (as shown in the Appendix). These limitations are inherent to PINN in handling high-gradient fields (Cuomo et al., 2022; Karniadakis et al., 2021), and as such, results for randomly distributed inclusions are not included in this manuscript. It is noted that the key advantage of the proposed DHN method lies in its strong-form formulation, which directly enforces the governing equations at collocation points. This eliminates the need for assembling and solving large systems of equations based on tangent stiffness matrices in

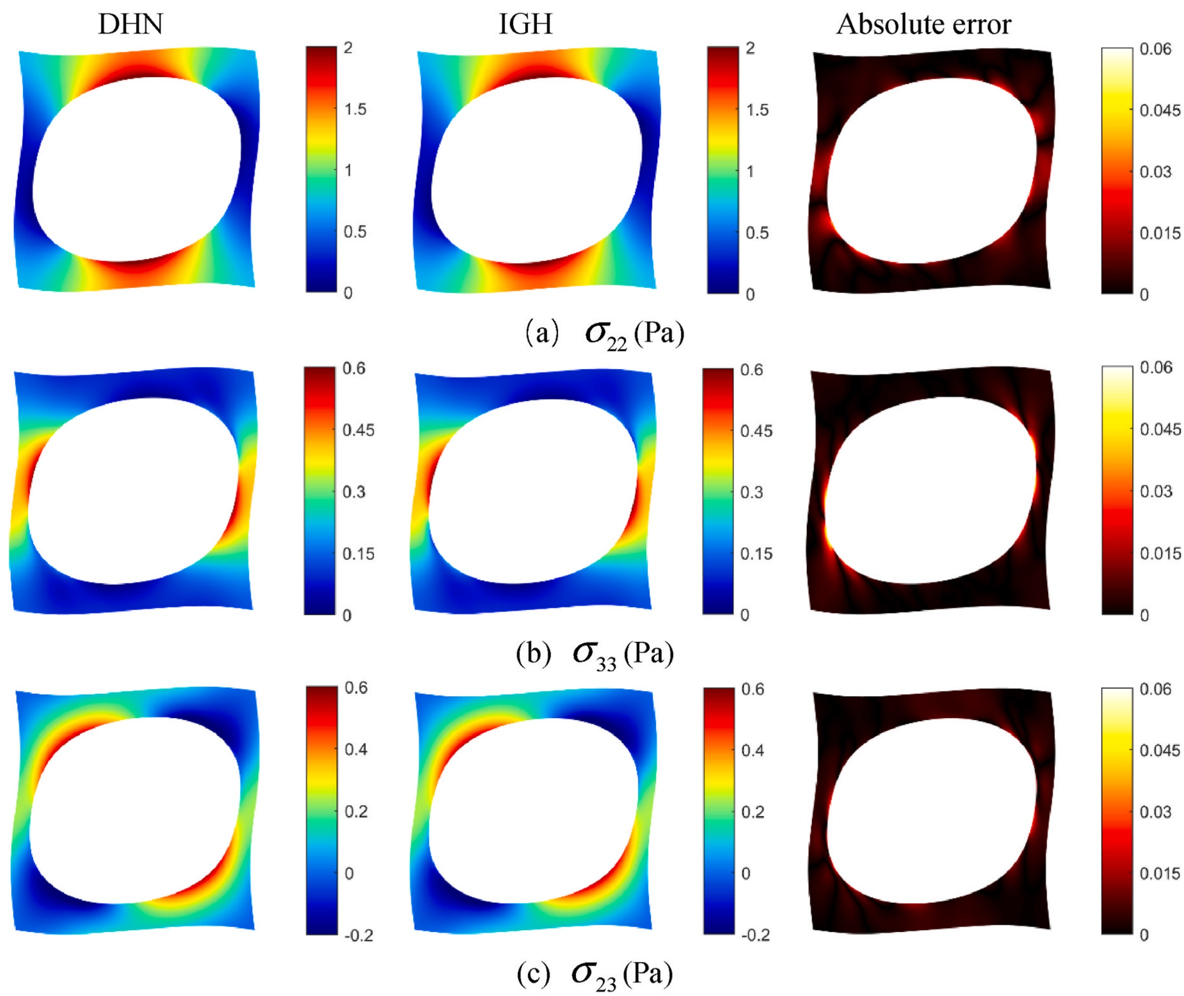

Fig. 17. Comparison of transverse normal σ_{22}, σ_{33} and shear σ_{23} stress distributions in square array of unidirectional pore with 35% pore content generated with the DHN and IGH method under non-proportional macroscopic displacement gradient $\overline{H}_{22} = 2\overline{H}_{23} = 0.5$

classical numerical solutions. As a result, our method offers a mesh-free and formulation-independent approach, particularly well-suited for exploring nonlinear micromechanics problems where the material behavior is complex and the governing equations may evolve. Furthermore, the proposed DHN method makes micromechanical modeling more accessible and user-friendly, particularly for researchers and engineers who may not have in-depth knowledge of traditional homogenization techniques. It provides a practical alternative for obtaining both the overall and local responses of periodic composites under finite strains. In this sense, it opens up the study of micromechanics to a broader community.

4.1. Fibrous materials

First of all, we consider a hexagonal array of unidirectional fiber in the matrix phase. We apply an in-plane macroscopic displacement gradient $\overline{H}_{22} = 0.5$. The fiber volume fraction is 20%. Fig. 3 depicts the distribution of collocation points used in the loss function, where the fiber (red) and matrix (blue) collocation points are randomly generated through Monte Carlo simulations, while the interface collocation points (black) are uniformly distributed along the fiber/matrix boundary. A total of 8000, 2000, and 360 points are assigned to the fiber, matrix, and interface phases, respectively. We employ a dual-neural network model, wherein each neural network architecture is 2-30-30-30-30-2. The sigmoid function is used as the activation function unless stated otherwise. The initial learning rates for both the network parameters and adaptive weights are 0.05, reducing by 50% after every 3000 steps. The learning rates associated with adaptive weights are reset to zero once 15000 training epochs are completed. Initially, the adaptive weights related to the PDEs and interfacial traction loss are both assigned a value of 1.

Fig. 4 compares the evolution of bulk loss (i.e. unweighted loss for the PDEs residuals in the fiber and matrix domain), interface loss (i.e. unweighted loss for the continuity residuals in displacement and tractions), and the weighted cumulative loss as a function of training epochs. We find that the loss value nearly converges to a constant after 20,000 training epochs. Fig. 5 shows the evolution of averaged collocation point weights as a function of training epochs. We observe that the final average weight for the PDEs loss is 46.8 times higher than its initial value, while the final average weight for the continuity loss is 13.5 times higher than its initial value. Fig. 6 illustrates pointwise distributions of adaptive weights in the unit cell. It should be noted that the neural network automatically learns higher weights near the interface, where high-stress concentrations are expected.

Fig. 7 compares the predictions of microscopic displacements u_2' and u_3' and the absolute differences generated with the finite-deformation DHN and IGH theories under macroscopic displacement gradient $\overline{H}_{22} = 0.5$. It is observed that the DHN results exhibit a high degree of accordance with the IGH results. Fig. 8 shows the comparison of concomitant stress σ_{22}, σ_{33} and σ_{23} distributions by the two approaches. While in the fiber phase the normal stresses remain nearly uniform and the shear is zero, the stresses in the matrix phase exhibit significant variations. Particularly worthy of notice is that the DHN technique captures

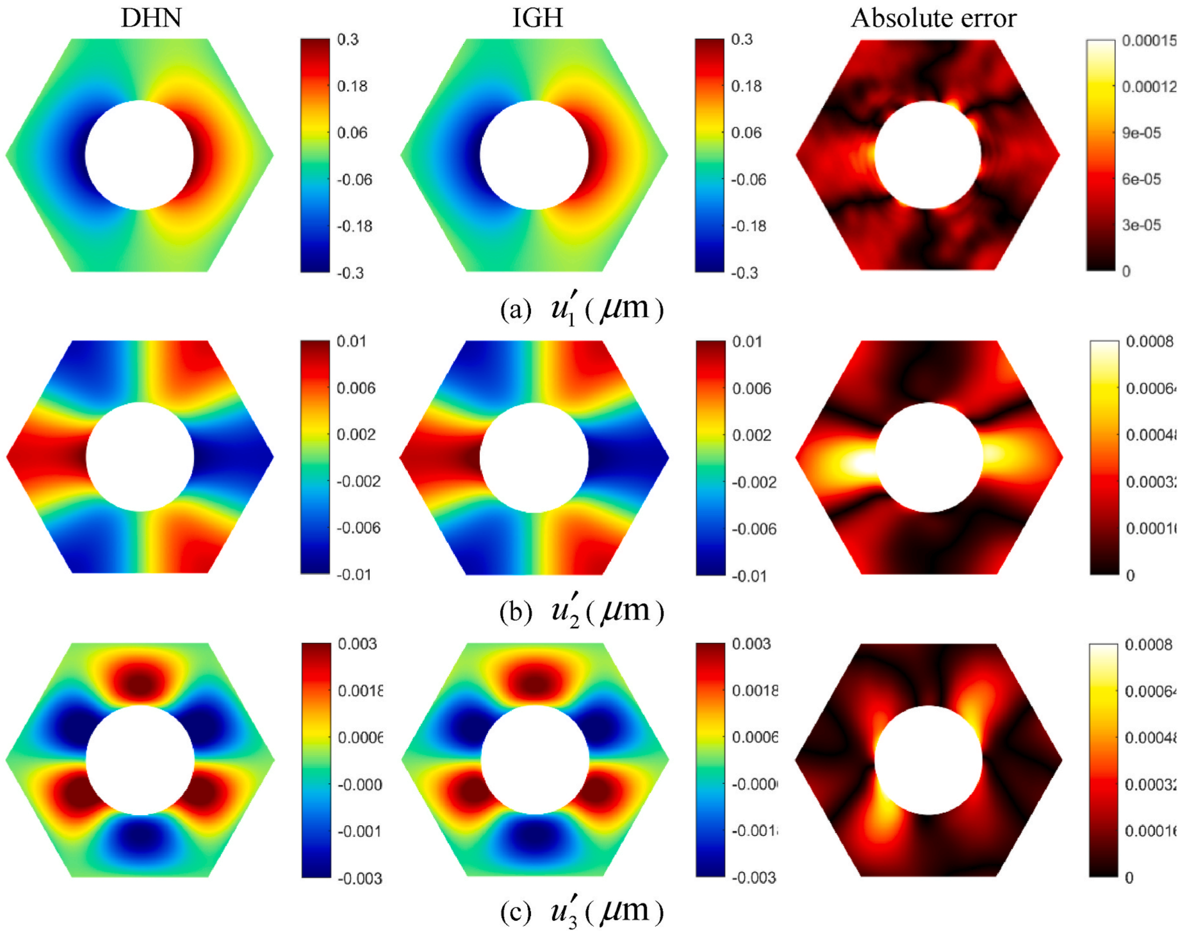

Fig. 18. Comparison of fluctuating displacements u_1', u_2', u_3' distributions in hexagonal array of unidirectional pore with 20% pore content generated with the DHN and IGH method under macroscopic displacement gradient $\overline{H}_{12} = 0.5$

accurately the stress concentration in the vicinity of the interface. In summary, the DHN and IGH methods yield nearly identical local stress distributions, providing robust confirmation of the proposed approach's accuracy.

We note that to obtain the results in Figs. 7–8, the training of the DHN model took 7159s (averaged on three runs), whereas the in-house IGH took only 699s. These simulations were performed on a personal computer with 13th Gen Intel(R) Core (TM) I9–13900H @ 2.60 GHz, 32 GB memory, NVIDIA @ RTX TM4070 GPU, 24 GB memory, 64-bit operating system, and x64-based processor. The longer execution time of the DHN approach stems from its formulation, which transforms the unit cell problem into a nonlinear optimization problem with a rough loss landscape. Gradient-based optimization within this landscape is computationally intensive.

As shown in Fig. 9, to demonstrate the effect of collocation point density on neural network accuracy, we consider a hexagonal unit cell with a substantially coarser distribution of material points, namely, 1000 material points in the fiber/matrix domain and 36 points at the interface. Fig. 10 compares the DHN-predicted in-plane stress distributions obtained using this coarse distribution versus the original collocation point arrangement. The results clearly indicate that, despite the systematic reduction in material points entering the loss function, the key characters of the stress distributions are not fundamentally altered.

Next, we consider a square array of circular fiber in the matrix phase. We apply a macroscopic displacement gradient $\overline{H}_{23} = 0.5$. The fiber volume fraction is kept at 20%. Fig. 11 presents comparisons of fluctuating displacements u_2' and u_3' generated with the DHN and IGH theories. Fig. 12 compares the corresponding transverse normal and shear stress distributions σ_{22}, σ_{33}, σ_{23} by the two approaches. Once again, remarkable correlations are observed in the predicted full-field stress distributions.

In support of the DHN theory's ability to accurately reproduce local field variables at high volume content, we consider a hexagonal array of unidirectional fibers with 50% volume fraction. Fig. 13 illustrates the comparisons of fluctuating displacement u_2', u_3' distributions generated with the DHN and IGH methods under macroscopic displacement gradient $\overline{H}_{23} = 0.5$. Fig. 14 shows transverse normal and shear stress σ_{22}, σ_{33}, σ_{23} distributions under this loading condition. The large fiber volume compared to the overall unit cell size leads to considerable fiber-fiber interactions, resulting in markedly different stress fields in both the fiber and matrix phases. The fluctuating displacements generated by the DHN method align closely with the IGH benchmark results, offering strong evidence for the accuracy of the developed DHN approach.

4.2. Porous materials

We proceed to examine the predictive and modelling capabilities of

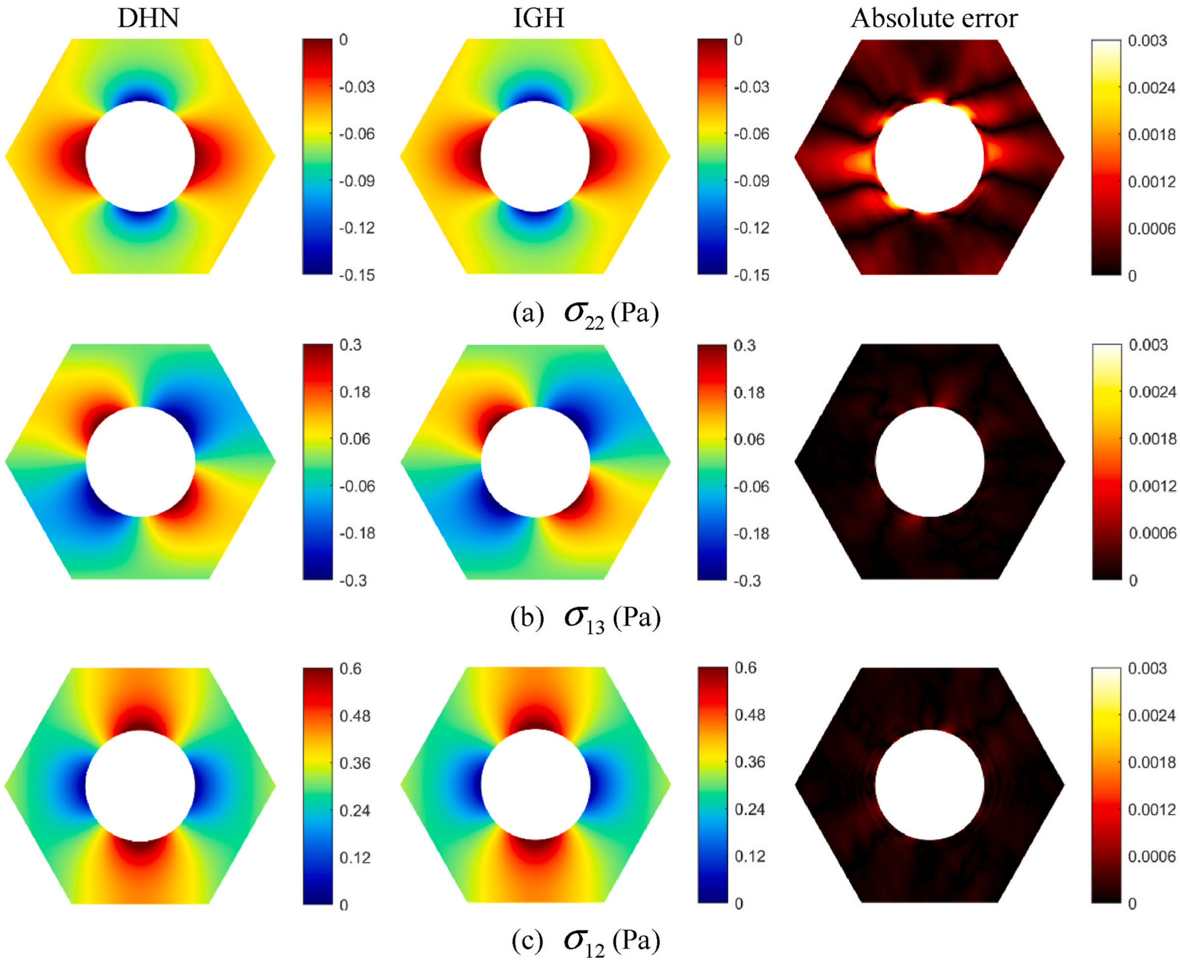

Fig. 19. Comparison of selected stress σ_{22}, σ_{13}, σ_{12} distributions in hexagonal array of unidirectional pores with 20% pore content generated with the DHN and IGH method under macroscopic displacement gradient $\overline{H}_{12} = 0.5$

the proposed DHN theory for periodic microstructures when the fibers are removed from the matrix phase, hence forming porous materials. The interfacial traction and displacement continuity conditions are replaced by the traction-free conditions along the pore boundary. Porosity significantly impacts the local stress distributions within the matrix phase compared to those reinforced with elastic fibers, leading to substantial deformation and pronounced stress concentrations around the pore interface. Hence, this system is a good candidate to assess the DHN's ability to capture the nonlinear material behavior under large deformation.

We consider a hexagonal array of cylindrical porosity with 50% volume fraction and apply the in-plane macroscopic displacement gradient $\overline{H}_{22} = 0.5$. The fluctuating displacements u'_2, u'_3 distributions and transverse normal and shear stresses σ_{22}, σ_{33}, σ_{23}, generated with the DHN and the IGH approaches, are compared in Figs. 15 and 16, respectively. Cursory examination of Figs. 15–16 reveals an excellent agreement between the DHN and IGH results.

To further assess the robustness of the DHN method, Fig. 17 compares the DHN- and IGH-predicted in-plane stress σ_{22}, σ_{33}, σ_{23} distributions in square array of unidirectional porosity with 35% pore content. Multi-axial displacement gradients $\overline{H}_{22} = 2\overline{H}_{23} = 0.5$ were applied. As anticipated, the DHN and IGH results show remarkable agreement, suggesting that the proposed DHN can be applied to non-proportional loading scenarios.

In the last example, we examine a hexagonal array of cylindrical porosity with 20% volume content and apply the out-of-plane macroscopic displacement gradient $\overline{H}_{12} = 0.5$. Fig. 18 presents comparison of the DHN's fluctuating displacements u'_1, u'_2, u'_3 with the IGH results. Fig. 19 shows the selected stress components σ_{22}, σ_{13}, σ_{12} distributions generated with DHN and IGH approaches. Similar to the preceding simulations, no visual differences between the DHN and IGH simulations are observed for this loading case.

5. Summary and conclusions

Computational homogenization techniques for soft composites depend on solving a system of partial differential equations with periodic boundary conditions. A recent trend in micromechanics simulation of these materials suggests replacing conventional numerical techniques with PINN solvers. Nevertheless, compared to the classical numerical methods, the standard PINN does not show clear advantages in terms of training accuracy, as it struggles to minimize the loss function that includes multiple loss terms. Therefore, a novel physics-informed deep homogenization approach is introduced for the localization of soft composites with periodic microstructures. Specific loss functions are constructed incorporating intricate knowledge of finite strain homogenization theory. A key feature of the proposed framework is that it directly solves the governing partial differential equations in terms of the first Piola-Kirchhoff stress using neural networks, thereby eliminating the need for iterative solutions of the nonlinear equations defined by the residual vector and tangent matrix. Additionally, a multi-network architecture has been proposed, where distinct neural networks are employed for each phase of the composite—a crucial improvement that enhances the model's ability to capture solution discontinuities across the fiber/matrix interface. Moreover, the proposed neural network framework satisfies exactly the periodicity boundary conditions of both tractions and displacements for hexagonal and square periodic microstructures. The proposed framework offers three attractive advantages over classical numerical methods. First, its extension to the finite deformation regime is straightforward, as the strong-form momentum balance equations are directly solved using automatic differentiation within modern machine learning libraries, eliminating the need for mesh refinement required in weak-form solutions. Secondly, the approach eliminates the need for incremental solutions to the unit cell problem, directly computing the local fields for any given macroscopic deformation gradient in a single step. Thirdly, it allows for the seamless integration of arbitrary strain-energy density functions with minimal modifications, enhancing its flexibility for various material models.

We validated the proposed DHN framework with the IGH analysis on periodic arrays of unidirectional fibers/porosities. The constituent phases are described using the generalized Mooney-Rivlin materials, with the elastic fiber being ten times stiffer than the matrix phase. We tested the DHN method under transverse normal and shear, biaxial transverse normal and shear, and anti-plane shear loading scenarios. To showcase the versatility of the proposed method across different periodic microstructures, we considered a range of microstructural configurations, including porous media and reinforced hyperelastic solids in hexagonal and square arrays. These configurations span intermediate to high volume fractions (20%, 35%, 50%) to effectively capture the fiber-fiber and pore-pore interactions. We find that the proposed DHN framework exhibits a high level of correlation with the IGH results, demonstrating the potential of the use of the PINN for solving the finite deformation response of periodic microstructures.

CRediT authorship contribution statement

Qiang Chen: Writing – original draft, Software, Methodology, Investigation, Formal analysis, Conceptualization. **Xiaoxiao Du:** Writing – review & editing, Validation, Supervision, Methodology, Investigation, Formal analysis, Conceptualization. **George Chatzigeorgiou:** Writing – review & editing, Validation, Methodology, Investigation, Formal analysis. **Fodil Meraghni:** Writing – review & editing, Validation, Methodology, Investigation, Formal analysis. **Gang Zhao:** Writing – review & editing, Methodology, Investigation, Formal analysis. **Zhibo Yang:** Writing – review & editing, Visualization, Methodology, Investigation, Formal analysis.

Declaration of competing interest

The authors declare that they have no known competing financial interests or personal relationships that could have appeared to influence the work reported in this paper.

Acknowledgment

Qiang Chen acknowledges the financial support of the National Key Research and Development Program of China (Grant No. 2024YFB4609000). Zhibo Yang acknowledges the financial support of the National Natural Science Foundation of China (Grant No. 92360306).

Appendix

To examine the proposed DHN approach's capability in addressing the unit cell problem with sharp stress and deformation gradients, we consider a unit cell with 5 locally irregular pores, with a total pore volume fraction of 20%. We apply a macroscopic displacement gradient of $\overline{H}_{22} = 0.5$. Fig. 1A shows the training loss as a function of training epochs. As observed, the significant pore-pore interactions in this configuration lead to persistently high loss values, indicating that the neural network approach struggled to converge to the FEM solutions during training. Fig. 2A shows comparison of transverse normal stress σ_{22} distributions generated with the FEM and DHN methods. The neural network fails to predict the local stress concentration in the vicinity of the pores, yielding almost uniform stress fields in the bulk domain.

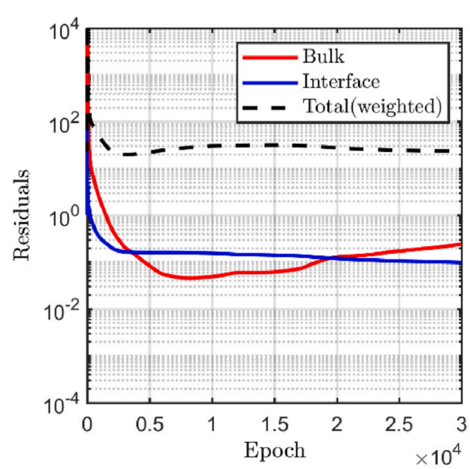

Fig. 1A. Training loss function in the case of multiple pores

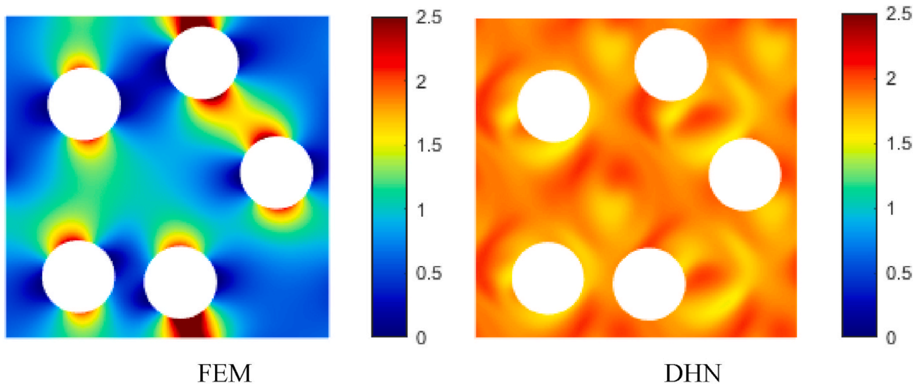

Fig. 2A. Comparison of the transverse normal stress σ_{22}(Pa) distributions generated with the FEM and DHN methods

Data availability

Data will be made available on request.

References

Abueidda, D.W., Koric, S., Al-Rub, R.A., Parrott, C.M., James, K.A., Sobh, N.A., 2022. A deep learning energy method for hyperelasticity and viscoelasticity. Eur. J. Mech. Solid. 95, 104639.

Abueidda, D.W., Lu, Q., Koric, S., 2021. Meshless physics-informed deep learning method for three-dimensional solid mechanics. Int. J. Numer. Methods Eng. 122, 7182–7201.

Bensoussan, A., Lions, J.-L., Papanicolaou, G., 1978. Asymptotic Analysis for Periodic Structures. North Holland, Amsterdam,Netherlands.

Brodnik, N.R., Muir, C., Tulshibagwale, N., Rossin, J., Echlin, M.P., Hamel, C.M., Kramer, S.L.B., Pollock, T.M., Kiser, J.D., Smith, C., Daly, S.H., 2023. Perspective: machine learning in experimental solid mechanics. J. Mech. Phys. Solid. 173, 105231.

Cavalcante, M.A.A., Pindera, M.-J., 2013. Generalized FVDAM theory for periodic materials undergoing finite deformations—part II: results. J. Appl. Mech. 81.

Chen, Q., Chatzigeorgiou, G., Meraghni, F., Chen, X., Yang, Z., 2025. Physics-informed deep homogenization approach for random nanoporous composites with energetic interfaces. Eng. Appl. Artif. Intell. 140, 109735.

Chen, Q., Du, X., Wang, W., Chatzigeorgiou, G., Meraghni, F., Zhao, G., 2023. Isogeometric homogenization of viscoelastic polymer composites via correspondence principle. Compos. Struct. 323, 117475.

Chen, Q., Pindera, M.-J., 2020. Homogenization and localization of elastic-plastic nanoporous materials with Gurtin-Murdoch interfaces: an assessment of computational approaches. Int. J. Plast. 124, 42–70.

Chen, Q., Wang, G., Pindera, M.-J., 2018. Homogenization and localization of nanoporous composites-A critical review and new developments. Compos. B Eng. 155, 329–368.

Cruz-González, O.L., Rodríguez-Ramos, R., Otero, J.A., Ramírez-Torres, A., Penta, R., Lebon, F., 2020. On the effective behavior of viscoelastic composites in three dimensions. Int. J. Eng. Sci. 157, 103377.

Cuomo, S., Di Cola, V.S., Giampaolo, F., Rozza, G., Raissi, M., Piccialli, F., 2022. Scientific machine learning through physics–informed neural networks: where we are and what's next. J. Sci. Comput. 92, 88.

Dong, S., Ni, N., 2021. A method for representing periodic functions and enforcing exactly periodic boundary conditions with deep neural networks. J. Comput. Phys. 435, 110242.

Du, X., Chen, Q., Chatzigeorgiou, G., Meraghni, F., Zhao, G., Chen, X., 2024. Nitsche's method enhanced isogeometric homogenization of unidirectional composites with cylindrically orthotropic carbon/graphite fibers. Compos. Sci. Technol. 256, 110787.

Du, X., Zhao, G., Wang, W., Fang, H., 2020. Nitsche's method for non-conforming multipatch coupling in hyperelastic isogeometric analysis. Comput. Mech. 65, 687–710.

El Fallaki Idrissi, M., Pasquale, A., Meraghni, F., Praud, F., Chinesta, F., 2025. Advanced meta-modeling framework combining machine learning and model order reduction towards real-time virtual testing of woven composite laminates in nonlinear regime. Compos. Sci. Technol. 262, 111055.

El Fallaki Idrissi, M., Praud, F., Meraghni, F., Chinesta, F., Chatzigeorgiou, G., 2024. Multiscale thermodynamics-informed neural networks (MuTINN) towards fast and frugal inelastic computation of woven composite structures. J. Mech. Phys. Solid. 186, 105604.

Gajek, S., Schneider, M., Böhlke, T., 2020. On the micromechanics of deep material networks. J. Mech. Phys. Solid. 142, 103984.

Haghighat, E., Raissi, M., Moure, A., Gomez, H., Juanes, R., 2021. A physics-informed deep learning framework for inversion and surrogate modeling in solid mechanics. Comput. Methods Appl. Mech. Eng. 379, 113741.

Henkes, A., Wessels, H., Mahnken, R., 2022. Physics informed neural networks for continuum micromechanics. Comput. Methods Appl. Mech. Eng. 393, 114790.

Hughes, T.J.R., Cottrell, J.A., Bazilevs, Y., 2005. Isogeometric analysis: CAD, finite elements, NURBS, exact geometry and mesh refinement. Comput. Methods Appl. Mech. Eng. 194, 4135–4195.

Jiang, J., Wu, J., Chen, Q., Chatzigeorgiou, G., Meraghni, F., 2023. Physically informed deep homogenization neural network for unidirectional multiphase/multi-inclusion thermoconductive composites. Comput. Methods Appl. Mech. Eng. 409, 115972.

Jiang, J., Zhao, J., Pang, S., Meraghni, F., Siadat, A., Chen, Q., 2022. Physics-informed deep neural network enabled discovery of size-dependent deformation mechanisms in nanostructures. Int. J. Solid Struct. 236–237, 111320.

Karniadakis, G.E., Kevrekidis, I.G., Lu, L., Perdikaris, P., Wang, S., Yang, L., 2021. Physics-informed machine learning. Nat. Rev. Phys. 3, 422–440.

Khatam, H., Pindera, M.-J., 2012. Microstructural scale effects in the nonlinear elastic response of bio-inspired wavy multilayers undergoing finite deformation. Compos. B Eng. 43, 869–884.

Kim, N.-H., 2015. Finite element analysis for nonlinear elastic systems. In: Kim, N.-H. (Ed.), Introduction to Nonlinear Finite Element Analysis. Springer US, New York, NY, pp. 141–239.

Linghu, J., Gao, W., Dong, H., Nie, Y., 2024. Higher-order multi-scale physics-informed neural network (HOMS-PINN) method and its convergence analysis for solving elastic problems of authentic composite materials. J. Comput. Appl. Math., 116223

Masi, F., Stefanou, I., 2022. Multiscale modeling of inelastic materials with Thermodynamics-based Artificial Neural Networks (TANN). Comput. Methods Appl. Mech. Eng. 398, 115190.

Masi, F., Stefanou, I., 2023. Evolution TANN and the identification of internal variables and evolution equations in solid mechanics. J. Mech. Phys. Solid. 174, 105245.

Masi, F., Stefanou, I., Vannucci, P., Maffi-Berthier, V., 2021. Thermodynamics-based Artificial Neural Networks for constitutive modeling. J. Mech. Phys. Solid. 147, 104277.

McClenny, L.D., Braga-Neto, U.M., 2023. Self-adaptive physics-informed neural networks. J. Comput. Phys. 474, 111722.

Nazem, M., Moavenian, M.H., 2021. Alternative remeshing techniques for large deformation analysis of geotechnical problems. Comput. Geotech. 138, 104344.

Nemat-Nasser, S., 1999. Averaging theorems in finite deformation plasticity. Mech. Mater. 31, 493–523.

Nguyen-Thanh, V.M., Anitescu, C., Alajlan, N., Rabczuk, T., Zhuang, X., 2021. Parametric deep energy approach for elasticity accounting for strain gradient effects. Comput. Methods Appl. Mech. Eng. 386, 114096.

Nguyen-Thanh, V.M., Zhuang, X., Rabczuk, T., 2020. A deep energy method for finite deformation hyperelasticity. Eur. J. Mech. Solid. 80, 103874.

Niu, S., Zhang, E., Bazilevs, Y., Srivastava, V., 2023. Modeling finite-strain plasticity using physics-informed neural network and assessment of the network performance. J. Mech. Phys. Solid. 172, 105177.

Raissi, M., Perdikaris, P., Karniadakis, G.E., 2019. Physics-informed neural networks: a deep learning framework for solving forward and inverse problems involving nonlinear partial differential equations. J. Comput. Phys. 378, 686–707.

Ren, X., Lyu, X., 2024. Mixed form based physics-informed neural networks for performance evaluation of two-phase random materials. Eng. Appl. Artif. Intell. 127, 107250.

Roy, A.M., Guha, S., Sundararaghavan, V., Arróyave, R., 2024. Physics-infused deep neural network for solution of non-associative Drucker–Prager elastoplastic constitutive model. J. Mech. Phys. Solid. 185, 105570.

Saeb, S., Steinmann, P., Javili, A., 2016. Aspects of computational homogenization at finite deformations: a unifying review from reuss' to Voigt's bound. Appl. Mech. Rev. 68, 050801.

Samaniego, E., Anitescu, C., Goswami, S., Nguyen-Thanh, V.M., Guo, H., Hamdia, K., Zhuang, X., Rabczuk, T., 2020. An energy approach to the solution of partial

differential equations in computational mechanics via machine learning: concepts, implementation and applications. Comput. Methods Appl. Mech. Eng. 362, 112790.
Sekkal, S.E., El Fallaki Idrissi, M., Meraghni, F., Chatzigeorgiou, G., Chinesta, F., 2025. Multiscale thermodynamics-informed neural networks (MuTINN) for nonlinear structural computations of recycled thermoplastic composites. Compos. B Eng. 300, 112455.
Suquet, P.M., 1987. Introduction. In: Sanchez-Palencia, E., Zaoui, A. (Eds.), Homogenization Techniques for Composite Media. Springer Berlin Heidelberg, Berlin, Heidelberg, pp. 193–198.
Tran, H., Gao, Y.F., Chew, H.B., 2024. Numerical and experimental crack-tip cohesive zone laws with physics-informed neural networks. J. Mech. Phys. Solid. 193, 105866.
Wu, J., Chen, Q., Jiang, J., Chatzigeorgiou, G., Meraghni, F., 2024. Adaptive deep homogenization theory for periodic heterogeneous materials. Compos. Struct. 340, 118171.
Wu, J., Jiang, J., Chen, Q., Chatzigeorgiou, G., Meraghni, F., 2023. Deep homogenization networks for elastic heterogeneous materials with two- and three-dimensional periodicity. Int. J. Solid Struct. 284, 112521.
Zhao, W., Hao, R., Zhang, M., Chen, Q., Yang, Z., Chen, X., 2025. Physically informed neural networks for homogenization and localization of composites with periodic microstructures. Compos. Struct. 367, 119260.